Plume Fragmentation by Bulk Interactions in Turbulent Rayleigh-Bénard Convection

Johannes Bosbach, Stephan Weiss, and Guenter Ahlers

Phys. Rev. Lett. **108**, 054501 — Published 1 February 2012

DOI: 10.1103/PhysRevLett.108.054501

Plume fragmentation by bulk interactions in turbulent Rayleigh-Bénard convection

Johannes Bosbach[1,2], Stephan Weiss[1], and Guenter Ahlers[1]
[1] *Department of Physics, University of California, Santa Barbara, CA 93106, USA and*
[2] *Institute of Aerodynamics and Flow Technology, German Aerospace Center (DLR), Göttingen, 37073, Germany*
(Dated: December 5, 2011)

Using compressed gases with Prandtl numbers near 0.7, we obtained flow visualizations of turbulent Rayleigh-Bénard convection in a cylindrical sample with an aspect ratio $\Gamma \equiv D/L \cong 10$ (D is the diameter and L the height) by the shadowgraph method. Focusing on the plumes under the top plate, we found that their length had a log-normal distribution, suggesting a fragmentation process. Fragmentation events could be visually identified in the images and involved plume interactions with bulk fluctuations or upwelling domain walls. We found the mean spacing between plumes to vary with the Rayleigh number in proportion to the volume-averaged Kolmogorov length of the turbulent bulk fluctuations, providing further evidence for plume-bulk interactions.

PACS numbers: 47.27.te,47.20.Bp,47.27.Cn,47.27.De

Turbulent flows generally are characterized by the time and length scales of their spatial structures. Here we examine certain length scales characteristic of plumes that form in turbulent convection of a fluid confined between two horizontal parallel plates separated by a distance L and heated from below (Rayleigh-Bénard convection or RBC, for reviews see [1–3]). This work is of interest for two reasons. On the one hand, whereas time scales have been examined extensively [3] in this system, only very little is known from experiment or direct numerical simulation (DNS) about length scales because it has been difficult to produce turbulent flows in samples of sufficient lateral size for their study. On the other, understanding plume dynamics and the probability distributions of their properties is important because plumes are major local contributors to the global heat transport; and a deeper understanding of plume properties and dynamics can be expected to shed light on the heat-transport mechanism.

In agreement with previous work [4–8], we found that the length of plumes near the top plate of the sample is log-normal distributed, suggesting that plumes are fragmented structures [9–11]. Here we provide evidence for interactions between the plumes on the one hand and bulk structures, such as domain walls and velocity or temperature fluctuations, on the other, and suggest that this interaction is the cause of the fragmentation. We were able to visually identify fragmentation events that led to the breakup of each of many longer plumes into two shorter ones due to interactions with excitations in the bulk fluid. We also found that the inverse total plume length $1/L_{pl}$, and thus the mean spacing between plumes, had a power-law dependence on the dimensionless temperature difference known as the Rayleigh number Ra (see below) with an exponent of 0.34 ± 0.03. This exponent is the same within our resolution as $\zeta_{eff} = 0.34$ which describes the volume-averaged Kolmogorov length (see, for instance, [13]); this length is related to fluctuations in the bulk. Our result differs from the exponent $\gamma_{eff} = 0.28$ of the thermal boundary-layer thickness λ_b or the Nusselt number Nu, which often have been assumed to be central in determining plume properties. This finding again suggests that the bulk fluctuations play a significant role in determining the plume statistics.

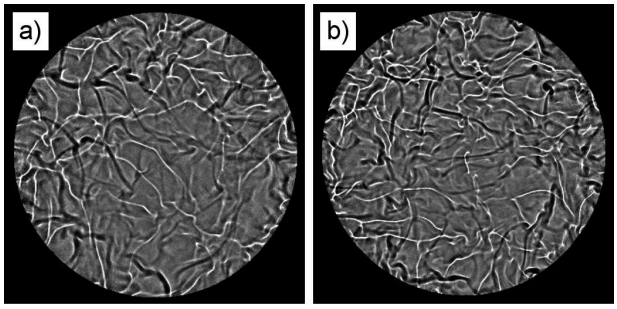

FIG. 1: Shadowgraph images for N_2 and (a) $\mathrm{Ra} = 6.8 \times 10^5$, P = 18.62 bars and (b) $\mathrm{Ra} = 1.1 \times 10^6$, P = 26.20 bars. The image diameter is equal to 77% of the sample diameter.

In turbulent RBC there are two thermal boundary layers (BLs), one below the top and the other above the bottom plate. Approximately half of the applied temperature difference ΔT is found across each BL, with the interior at nearly uniform temperature in the time average but containing strong temperature and velocity fluctuations. The BLs adjust their thicknesses λ_b so as to be close to their marginal stability [14–16], thus providing an example of self-organized criticality [17, 18]. As they fluctuate across the stability curve, they emit volumes of relatively hot (cold) fluid known as "plumes" at the bottom (top) of the sample at random time intervals and at irregular locations. Initially these plumes are one-dimensional excitations [6, 19] and thus we refer to them as line plumes [19]. They tend to stay near the BL from which they are emitted, and are carried laterally by global flows known as the large-scale circulation (LSC) when these are present. When they approach the side wall, or in a large enough sample a domain wall,

they typically rise or fall. Here we focused on relatively cold plumes that form under the top plate. They can be seen as relatively bright lines in Fig. 1. The plumes are one component of RBC turbulence; additional ones are the small-scale temperature and velocity fluctuations that exist throughout the bulk of the sample.

The Rayleigh number is $\mathrm{Ra} = \beta g \Delta T L^3/(\nu\kappa)$ where g is the acceleration of gravity, β is the isobaric thermal expansion coefficient, and κ and ν are the thermal diffusivity and the kinematic viscosity respectively. The Nusselt number is a dimensionless effective thermal conductivity and is given by $Nu = QL/(\Delta T\lambda)$. Here Q is the heat-current density and λ is the thermal conductivity. Finally, the Prandtl number is $Pr = \nu/\kappa$.

In the RBC problem there are two characteristic length scales that might be expected to determine spatial correlations. One of them is the thermal BL thickness [20, 21] which can be represented well by

$$\lambda_b = L/(2Nu) \sim \mathrm{Ra}^{-\gamma_{eff}} \ . \qquad (1)$$

Although λ_b is not directly involved in fluctuations, it may play a role in determining the width of line plumes and thus may have an indirect influence. The other more directly relevant scale is the coherence length, often defined as $l_{coh} = 10\eta_K$ [13, 22] where

$$\eta_K/L = Pr^{1/2}\,[Ra(Nu-1)]^{-1/4} \sim \mathrm{Ra}^{-\zeta_{eff}} \qquad (2)$$

is the volume-averaged Kolmogorov length [23]. The coherence length is an estimate of the smallest size of coherent structures, or eddies, in the bulk. One sees that, at constant Pr and for Nu >> 1,

$$\zeta_{eff} = (1+\gamma_{eff})/4 \ . \qquad (3)$$

Over our Ra and Pr range we have [24, 25] $\gamma_{eff} \simeq 0.28$. We estimate $\zeta_{eff} \simeq 0.34$, which is slightly larger than 0.32 given by Eq. 3 because in the experiment Pr increased slightly with Ra and because Nu was not large enough for Eq. 3 to apply quantitatively. The two length scales should be distinguishable by their dependence on Ra. At much larger Ra and Pr $\gtrsim 3$, γ_{eff} approaches 0.31 [25, 26] and thus the two length scales are more difficult to distinguish by their Ra dependences.

We used various gases under pressure which permitted reaching Ra values well in the turbulent range [12] with $L \simeq 1$cm. Thus we could construct a sample with an aspect ratio $\Gamma \equiv D/L \simeq 10$ (D is the diameter) which nonetheless was physically sufficiently small to image most of it. The apparatus was described before [26–30]. We installed a convection cell with $D = 101$ mm with a 19.1 mm thick sapphire top plate that permitted optical access from above to a circular region with a diameter of $0.82D$. The bottom plate was copper, with a 3.18 mm thick sapphire plate glued to its top surface. This sapphire had a thin layer of gold plated onto it

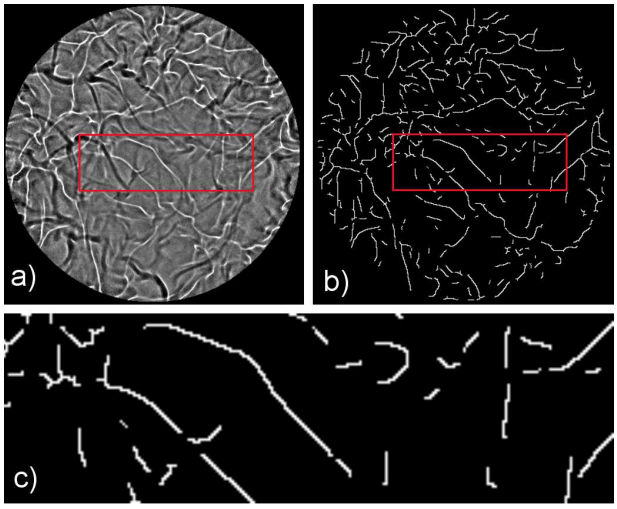

FIG. 2: Skeletonization of Fig. 1 (a). (a): Original divided image. (b): Skeletonized plume image. (c): Enlargement of the section in the rectangle in (a) and (b).

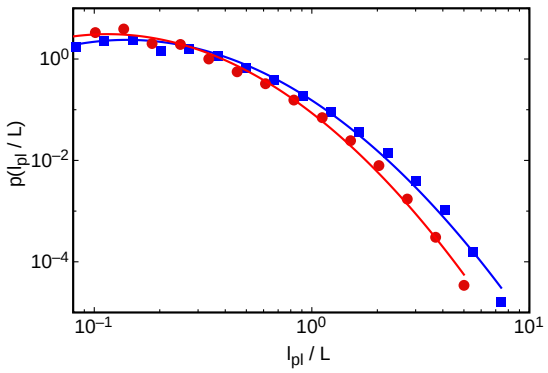

FIG. 3: Probability distribution $\mathrm{p}(l_\mathrm{pl}/L)$ of normalized plume lengths l_pl/L for $\mathrm{Ra} = 3.4 \times 10^5$ (solid squares, blue online) and $\mathrm{Ra} = 4.3\times10^6$ (solid circles, red online). The lines are fits of Eq. 4 to the data which yielded $a = 4.05$, $x_0 = 0.28$, $\sigma = 0.83$ for $Ra = 3.4 \times 10^5$ and $a = 12.3$, $x_0 = 0.22$, $\sigma = 0.81$ for $Ra = 4.3 \times 10^6$.

which provided a mirror needed for the shadowgraphy. The side walls were 1.55 mm thick high-tensile-strength stainless steel. The height was $L = 9.52$ mm, yielding $\Gamma = 10.6$. The sample was argon ($\mathrm{Pr} = 0.69$) or nitrogen ($\mathrm{Pr} = 0.73$) at pressures up to 50 bars. A shadowgraph tower [31] was mounted above the convection apparatus. Usually 1024 images were taken at a given Ra. All images were divided by a reference image obtained by averaging all images at the same Ra. Typical divided and rescaled images were shown in Fig. 1. We studied the turbulent range $3 \times 10^{-5} \lesssim \mathrm{Ra} \lesssim 5 \times 10^{-6}$ [12].

The bright structures were extracted from the images and skeletonized by reducing them to a width of a single pixel. An example of the result is shown in Fig. 2 for the image depicted in Fig. 1a. The distribution of the

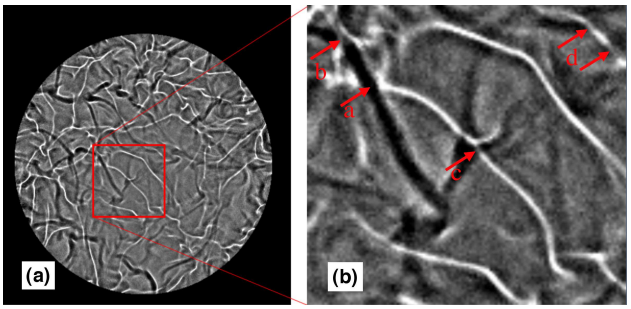

FIG. 4: Illustration of fragmentation events for Ra = 6.8×10^5. a): the same image as that in Fig. 1a. b): an enlargement of the section outlined by a square (red online) in the left image. Arrows (red online) point at fragmentation sites.

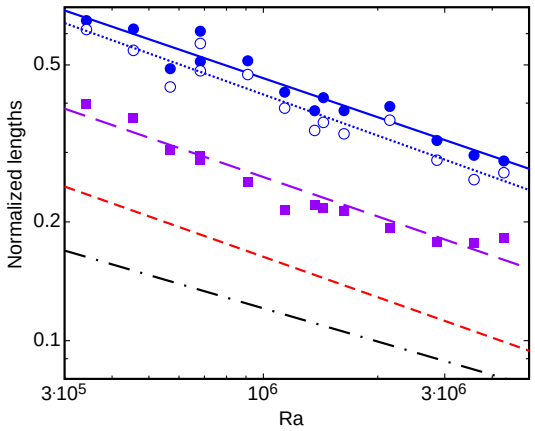

FIG. 5: Various normalized lengths as a function of Ra. Solid circles (blue online): Measured mean plume spacing $(A/L_{pl})/L$ (0.33 ± 0.03). Open circles (blue online): Mean plume spacing $(A/L_{pl}^{fit})/L$ based on Eq.6 (0.34 ± 0.03). Solid squares (purple online): Crossover wavelength l_{cross}/L of the regions of different exponents of the power spectra (see text) (0.33 ± 0.03). Dashed line (red online): coherence length $l_{coh}/L = 10\eta_K/L$ (0.34). Dash-dotted line: $2\lambda_b/L = 1/Nu$ (0.28). The number behind each item is the effective exponent from a power-law fit.

number of plumes of length l_{pl}/L as a function of l_{pl}/L was computed by counting the number of pixels in each bright structure. These distributions were averaged over all 1024 images at a given Ra. The result could be fitted with the log-normal distribution

$$P(x) = \frac{a}{x\sigma\sqrt{2\pi}} \exp[-\frac{(\ln(x) - \ln(x_0))^2}{2\sigma^2}] \ , \qquad (4)$$

$x = l_{pl}/L$, by adjusting the parameters a, x_0, and σ. Examples of the corresponding probability density functions $p(l_{pl}/L) = P(l_{pl}/L)/a$ and the fits by Eq. 4 are shown in Fig. 3. Since $p(l_{pl}/L = \Gamma) \lesssim 10^{-5}$, plumes with a length as large as the sample diameter are very rare, suggesting that the sample was large enough to reflect the properties of the infinite system.

Log-normal distributions were observed before for a number of plume properties [5–8]. The results in Fig. 3 can be compared directly with those in Fig. 17d of [6], which are for $\Gamma = 1.00$ and Pr = 5.4. For that Γ and Pr the range of about 1.3 decades of l_{pl}/L that was available nicely covered the peak (on logarithmic scales) of the distribution. For our larger $\Gamma \simeq 10$ even our somewhat larger range of l_{pl}/L of over two decades, if it is to cover the large end of the distribution where $l_{pl}/L \simeq \Gamma$, is still insufficient to also cover the short-plume range with $l_{pl}/L \lesssim 0.1$. Nonetheless the log-normal shape of our data is apparent, and more than 87 % of the plumes are accounted for in the accessible range $l_{pl}/L \gtrsim 0.09$. The change of the distribution with Pr and Ra (which is reflected in the parameters x_0 and σ) is small, but the total number of plumes, reflected in the parameter a, changed significantly with Ra [12].

Log-normal distributions are indicative of fragmentation processes. Of primary interest is the source of the fragmentation. Figure 4 shows an example that sheds light on this issue. Part (b) is an enlargement of the area identified by a square in (a); it contains several fragmentation events. Some of the events are pointed out by small arrows labeled by a letter (red online). Near the left upper corner of (b) a broad black diagonal line can be seen which we believe to be an upwelling domain wall. It divided a long white plume into two parts (event a) and did further damage to a shorter plume just above that fragmentation point (event b). In the center of (b) a seemingly more complex event (event c) is dividing the originally very long plume into more parts. In the upper right corner a fragmentation process (event d) seems to be in its early stages, with the original plume still intact but thinned at two places, this time most likely by bulk fluctuations. Many more fragmentation events due to interactions with domain walls or fluctuations can be identified in the entire image (a) as well as in all other images that we examined. On the basis of these observations we believe that bulk-plume interaction is the leading cause of the fragmentation reflected in the probability distributions shown in Fig. 3.

Further evidence for the influence of the bulk on the plume distribution comes from an examination of plume length scales. In Fig. 5 we show as solid circles (blue online) the mean spacing between plumes. It is defined here as the ratio (A/L_{pl}) between the sample area A and the total plume length L_{pl}, normalized by the sample height L. A power-law fit to the data yields an exponent of 0.33 ± 0.03, which agrees very well with the exponent $\zeta_{eff} = 0.34$ of l_{coh}/L but disagrees with the exponent $\gamma_{eff} = 0.28$ of λ_b.

The parameters obtained from the fits of Eq. 4 to the experimental distributions can be used to compute the average plume length (normalized by L)

$$l_{pl}^{fit}/L = \exp[\ln(x_0) + \sigma^2/2]] \qquad (5)$$

and the normalized total plume length

$$L_{pl}^{fit}/L = a l_{pl}^{fit}/L \ . \qquad (6)$$

The corresponding results for the plume spacing $(A/L_{pl}^{fit})/L$ are shown in Fig. 5 as open circles (blue online). They are slightly lower than the solid circles because they are based on the entire integral of the distribution function and thus include the very short plumes that were not accessible to direct measurement. A power-law fit to them yielded the exponent 0.34 ± 0.03, again in agreement with ζ_{eff}. It is interesting to note that this average spacing between plumes is only a factor of 2.6 (averaged over all Ra) larger than l_{coh}/L, suggesting that only very few fluctuations, if they occurred near the top plate, would find room between the plumes without significant interaction.

In order to obtain yet another typical length scale of the plumes, we computed the squares of the moduli of the two-dimensional Fourier transforms of the skeletonized plume images like the one in Fig. 2b, averaged them over the 1024 realizations at each Ra, and then computed the azimuthal averages $\mathcal{P}(q)$ (for details, see [12]). All spectra revealed a low-q section where $\mathcal{P}(q) \sim q^{-0.3}$, followed by a steeper section where $\mathcal{P}(q) \sim q^{-1.3}$ [12]. We believe that the exponents may be influenced by uncontrolled experimental effects, but the overall shape of $\mathcal{P}(q)$ with a well defined crossover between the two regimes is not unlike that of the Fourier transform of the second-order velocity structure function [3]. The crossover gives a well defined length scale l_{cross}/L which we show in Fig. 5 as solid squares (purple online). A power-law fit to these data yielded an exponent of 0.33 ± 0.03, again consistent with $\zeta_{eff} = 0.34$ and inconsistent with $\gamma_{eff} = 0.28$. Averaged over all Ra, we find $l_{coh}/l_{cross} = 0.63$, *i.e.* of order unity as one might expect [12].

The prevailing view of plume dynamics has been that plumes are born in the marginally stable thermal BLs as line plumes (RBC "rolls"), and that they tend to remain near the BLs but are swept laterally by a large-scale circulation (LSC) until cold (warm) plumes fall (rise) near a side wall when one is present. Near the wall, plumes (by virtue of their buoyancy) are believed to contribute to the driving of the LSC, and in turn are expected to be carried along by the LSC on their journey to the opposite plate while their shape evolves gradually by heat diffusion; recently it was suggested also that there is plume evolution due to plume-plume collision [6] in the regions near the side wall where the plume density tends to increase. This view of the plume dynamics does not contain any fragmentation mechanism that would lead to log-normal distributions of the various plume properties and thus is an incomplete picture. Here we showed that cold plumes, while they reside near the top plate, interact with *bulk* excitations including up-welling domain walls and bulk temperature and/or velocity fluctuations. Both the domain walls and the fluctuations repeatedly cut a plume into two plumes of shorter length. We believe that this fragmentation process is responsible for the log-normal distribution of plume lengths.

We found as well that the mean spacing between plumes varies as $\mathrm{Ra}^{\zeta_{eff}}$ where $\zeta_{eff} = 0.34$ is the exponent of a coherence length l_{coh} which describes the smallest fluctuating structures present in bulk RBC [13, 22], again indicating that the bulk has a strong influence on plume dynamics. Further, we found that, independent of Ra, the average spacing between plumes is only about two or three times l_{coh}, leaving little space for fluctuations in the bulk but near the plate without plume interaction. Thus, a picture emerges where the plume density, which corresponds to an average inter-plume distance of order l_{coh}, is determined by a competition between the rate of plume production in the BL and the rate of plume destruction by plume-bulk interactions, and not just by the plume emission-rate from the BL.

We note that our conclusion $(A/L_{pl})/L \propto \mathrm{Ra}^{-\zeta_{eff}}$ differs from the proposal of [7] which states that $(A/L_{pl})/L \propto \mathrm{Ra}^{-1/3}$ where the exponent 1/3 seems to have its origin in the assumption that there is a critical BL Rayleigh number Ra_c^{BL}, defined with L replaced by λ_b and ΔT by $\Delta T/2$, which is independent of Ra and which, *via* Eq. 1, leads to the estimate $\gamma_{eff} = 1/3$.

Acknowledgements: One of us (GA) acknowledges several very constructive conversations with D. Lohse. One of us (JB) gratefully acknowledges support by the "DLR Forschungssemester" of the German Aerospace Center. This work was supported by the U.S. National Science Foundation through Grant DMR07-02111.

[1] G. Ahlers, S. Grossmann, and D. Lohse, Rev. Mod. Phys. **81**, 503 (2009).
[2] G. Ahlers, Physics **2**, 74 (2009).
[3] D. Lohse and K.-Q. Xia, Annu. Rev. Fluid Mech. **42**, 335 (2010).
[4] B. Baburaj, A. Puthenveettil, and J. Arakeri, J. Fluid Mech. **542**, 217 (2005).
[5] Q. Zhou, C. Sun, and K.-Q. Xia, Phys, Rev. Lett. **98**, 074501 (2007).
[6] Q. Zhou and K.-Q. Xia, New J. Phys. **12**, 075006 (2010).
[7] B. A. Puthenveettil *et al.*, J. Fluid Mech. DOI:10.1017/jfm.2011.319 (2011).
[8] O. Shishkina and C. Wagner, J. Fluid Mech. **599**, 383 (2008).
[9] A. N. Kolmogorov, Dokl. Akad. Nauk SSSR **31**, 99 (1941).
[10] L. Oddershede, P. Dimon, and J. Bohr, Phys. Rev. Lett. **71**, 3107 (1993).
[11] E. Villermaux, Annu. Rev. Fluid Mech. **39**, 419 (2007).
[12] See Supplemental Material at [URL will be inserted by publisher] for a more detailed discussion of the onset of turbulence, of the dependence of the parameters in Eq. (4) on Ra, and of the spectral analysis of the plume density.
[13] K. Sugiyama, E. Calzavarini, S. Grossmann, and D. Lohse, Europhys. Lett. **80**, 34002 (2007).
[14] M. V. R. Malkus, Proc. R. Soc. London A **225**, 196 (1954).
[15] B. Castaing, J. Phys. **50**, 147 (1989).
[16] G. Zocchi, E. Moses, and A. Libchaber, Physica A **166**, 387 (1990).
[17] P. Bak, C. Tang, and K. Wiesenfeld, Phys. Rev. Lett. **59**, 381 (1987).
[18] P. Bak, C. Tang, and K. Wiesenfeld, Phys. Rev. A **38**, 364 (1988).
[19] D. Funfschilling, E. Brown, and G. Ahlers, J. Fluid Mech. **607**, 119 (2008).
[20] A. Belmonte, A. Tilgner, and A. Libchaber, Phys. Rev. Lett. **70**, 4067 (1993).
[21] A. Belmonte, A. Tilgner, and A. Libchaber, Phys. Rev. E **50**, 269 (1994).
[22] S. Grossmann and D. Lohse, Phys. Lett. A **173**, 58 (1993).
[23] A coherence length based on the *local* energy dissipation [3], averaged only near the vicinity of the top plate, would be more appropriate but is not available. We do not expect the final result to be very different.
[24] D. C. Threlfall, J. Fluid Mech. **67**, 17 (1975).
[25] S. Grossmann and D. Lohse, Phys. Rev. Lett. **86**, 3316 (2001).
[26] X. Xu, K. M. S. Bajaj, and G. Ahlers, Phys. Rev. Lett. **84**, 4357 (2000).
[27] G. Ahlers and X. Xu, Phys. Rev. Lett. **86**, 3320 (2001).
[28] A. Nikolaenko, E. Brown, D. Funfschilling, and G. Ahlers, J. Fluid Mech. **523**, 251 (2005).
[29] D. Funfschiling, E. Brown, A. Nikolaenko, and G. Ahlers, J. Fluid Mech. **536**, 145 (2005).
[30] J.-Q. Zhong, D. Funfschilling, and G. Ahlers, Phys. Rev. Lett. **102**, 124501 (2009).
[31] J. R. de Bruyn, E. Bodenschatz, S. W. Morris, S. Trainoff, Y. Hu, D. S. Cannell, and G. Ahlers, Rev. Sci. Instrum. **67**, 2043 (1996).